International Journal of Heat and Mass Transfer 52 (2009) 3955–3962

Contents lists available at ScienceDirect

International Journal of Heat and Mass Transfer

journal homepage: www.elsevier.com/locate/ijhmt

Source identification for unsteady atmospheric dispersion of hazardous materials using Markov Chain Monte Carlo method

Shaodong Guo [a,b], Rui Yang [a,*], Hui Zhang [a], Wenguo Weng [a], Weicheng Fan [a]

[a] Center for Public Safety Research, Department of Engineering Physics, Tsinghua University, Beijing 100084, China
[b] Department of Engineering Mechanics, School of Aerospace, Tsinghua University, Beijing 100084, China

ARTICLE INFO

Article history:
Received 12 December 2008
Accepted 23 March 2009
Available online 4 May 2009

Keywords:
Hazardous materials release
Source inversion
Bayesian inference
Unsteady adjoint equation
Adaptive mesh refinement

ABSTRACT

This paper is to study source inversion and identification of hazardous gas dispersion in a three-dimensional urban area. An unsteady adjoint transportation model was adopted, and an advanced numerical scheme based on adaptive mesh refinement was used. A time-dependent concentration database over the entire parameter space was generated. Markov Chain Monte Carlo sampling based on the Bayesian inference was used to invert the parameters such as source location and its strength obtained from the database at different sampling time of sensor readings and simulation results. The probability distributions of source parameters were calculated and predicted source location and strength agree well with actual values which indicates the feasibility of the proposed method and procedure. Numerical studies also show that the computational scheme is efficient when using unsteady adjoint transportation equation with MCMC methods. The unsteady inversion method proposed here can also improve the accuracy of source location in the wind direction compared with the steady inversion method for the case of atmospheric release of hazardous materials.

1. Introduction

Urban safety has received more attention recently due to the increased population and high possibility of terrorist attack involving release of hazardous CBR (chemical/biological/radiological) materials in a city. When the materials accidentally release in an urban center, it is critical to predict the transport characteristics of the plume so as to effectively make strategical planning for the management of emergency response. In general the atmospheric transport of hazardous CBR materials can be predicted through either analysis or simulations [1,2]. Spalding et al. have made tremendous contribution to computational fluid dynamics society through advancing and developing numerical methods for various industrial applications [3,4]. The most distinguished achievement is the development of well known computational software- PHOENICS. After Spalding's work, much development has also been made in the computational field to cater for various demands in applications. However, most developments were to tackle the known source location and strength. For the terrorist attack and other hazardous CBR agent release, source conditions are often unknown or limited. This requires the development of an efficient method to determine the source location and its strength from sensor network distributed in the city, combined with weather conditions such as wind velocity, direction and humidity, for rapid emergency response.

The source inverse modeling can be categorized into direct, optimized and probabilistic approaches. The direct approach solves heat conduction or mass transportation equation reversely to obtain the function or parameter estimation. The direct approach can be sub-categorized by analytical or numerical methods which have been applied to the development of inversion techniques in atmospheric constituent transport [5] and solving the inverse heat conduction problem (IHCP) [6–12]. The optimized method, has been used to seek the source parameters that is best-fitted through matching simulation and measurement. Different optimization techniques have been successfully used in the past for estimation of source parameters and functions [12–15]. The probabilistic approach has been used to obtain the probabilities of the source parameters in the region surrounding the critical point with introducing the measurement error and simulation error. An important probabilistic approach is within the Bayesian context. Wang et al. [16,17] used the Bayesian inference and Markov Chain Monte Carlo (MCMC) sampling for the solution of IHCP. Chow et al. [18] applied the Bayesian methodology to inverse the source for atmospheric release of hazardous CBR materials in the urban area. In general the method is time-consuming. To improve the efficiency, Keats et al. [19] introduced the adjoint equation to inverse the release source solving the concentration field. In practice in the early period of the release event, the concentration field is unsteady and the data from the sensors vary with time continuously. The dynamic

* Corresponding author.
E-mail address: ryang@tsinghua.edu.cn (R. Yang).

0017-9310/$ - see front matter © 2009 Elsevier Ltd. All rights reserved.
doi:10.1016/j.ijheatmasstransfer.2009.03.028

Nomenclature

C	forward concentration (kg/m^3)
D	diffusion coefficient (m^2/s)
F	modeled concentration (kg/m^3)
$F^{(t)}$	modeled data at time t (kg/m^3)
G	adjoint concentration (m^{-2})
N	length of the Markov chain
$p(X)$	prior probability of source parameters
$p(X\|Y)$	conditional probability of source parameters
$p(Y\|X)$	likelihood probability
$p(Y^{rep}\|Y)$	sampling distribution of Y^{rep}
Q	source release rate (kg/s)
R	sensor location (m)
S	source strength (kg/m^3 s)
T	true concentration (kg/m^3)
$T^{(t)}$	true data at time t (kg/m^3)
$\vec{V}$	velocity (m/s)
X	source parameter
X_a	the early segment of Markov chain
X_b	the late segment of Markov chain
x	source location in x direction (m)
Y	measurement concentration (kg/m^3)
Y^{rep}	hypothetical replications of the measurement data (kg/m^3)
$Y^{(t)}$	measurement data at time t (kg/m^3)
y	source location in y direction (m)
z	source location in z direction (m)
Greek symbols	
δ	the thinning interval
ρ	the degree of autocorrelation
ε	measurement error (kg/m^3)
σ_f	standard deviation of model error (kg/m^3)
σ_y	standard deviation of measurement error (kg/m^3)
θ	mean of the Markov chain

inversion is therefore essential for real-time identification of source. Johannesson et al. [20] proposed the Sequential Monte Carlo (SMC) method to inverse the unsteady dispersion process of atmospheric release. In their model, a rather simple Gaussian puff model is employed which results in an analytical solution for the adjoint equation. This simple model is however unable to characterize the complex flow field and special phenomenon of the concentration transportation in an urban area.

In this paper, an unsteady dispersion process of hazardous CBR materials release in an urban environment is studied. The Bayesian probabilistic approach is adopted to make three-dimensional dynamic inversion to obtain the source location and strength. To construct a transient concentration database over the entire parameter space, an unsteady adjoint transportation equation is solved numerically using finite volume method with adaptive mesh refinement.

2. Fundamentals of inversion model

The detailed fundamental of the Bayesian inversion model was provided by Chow et al. [18] and Keats et al. [19]. Following their work, an unsteady dispersion process and dynamic source inversion model are studied in this paper. For the completeness of the paper, some of the formulations are repeated here.

2.1. Bayesian inference

The Bayesian theorem is used to determine the possibility of an event X occurring conditional on another event Y. This possibility is called the posterior possibility distribution, which is related to the possibility of the event Y occurring conditionally on the fact that event X has occurred [18].

$$p(X|Y) = \frac{p(Y|X)\cdot p(X)}{p(Y)} \propto p(Y|X)\cdot p(X) \tag{1}$$

When the CBR source releases in an urban area, the concentration of the toxic gas can be measured from an array of sensors. From a Bayesian perspective, there is no fundamental distinction between the measurement data and the source parameters. They are all considered as random quantities. Let $\mathbf{X} = \{X_1, X_2, \cdots, X_i, \cdots, X_n\}$ denote the source parameter or missing data, and $\mathbf{Y} = \{Y_1, Y_2, \cdots, Y_i, \cdots, Y_m\}$ denote the observed data or measurement data. Then $p(X|Y)$ characterizes the conditional possibility distributions of the source parameters (location, strength, and so on) considering the measurement data from sensors distributed in the urban environment. $p(X)$ denotes the prior distribution of the source parameters which is determined through all available prior information. $p(Y|X)$ denotes the likelihood function [18,20].

2.2. Likelihood function and errors

From Eq. (1), the likelihood is an essential function which is related to the prior distribution and the posterior distribution through the likelihood of the discrepancy of the measurements from sensors and numerical predictions. The discrepancy can be obtained by difference from measurements and simulations, so uncertainty analysis can be performed. Let $Y^{(t)} = \{Y_1^{(t)}, Y_2^{(t)}, \cdots, Y_i^{(t)}, \cdots, Y_k^{(t)}\}$ denote the observed data at sensors at time t and let $F^{(t)} = \{F_1^{(t)}, F_2^{(t)}, \cdots, F_i^{(t)}, \cdots, F_k^{(t)}\}$ denote the predicted concentration at sensors at time t which are obtained through performing a forward dispersion calculation by a numerical model. Both measurements and simulations have errors. Let $T^{(t)} = \{T_1^{(t)}, T_2^{(t)}, \cdots, T_i^{(t)}, \cdots, T_k^{(t)}\}$ denote the true concentration value at sensors at time t. The observed data are assumed to be related to the true value as $Y_i^{(t)} = T_i^{(t)} + \varepsilon_i^{(t)}$, where $\varepsilon^{(t)} = \{\varepsilon_1^{(t)}, \varepsilon_2^{(t)}, \cdots, \varepsilon_i^{(t)}, \cdots, \varepsilon_k^{(t)}\}$ are the independent Gaussian distributed measurement errors with zero mean and a known standard deviation $\sigma_y^{(t)}$ at time t. So the observed data can be written as $Y_i^{(t)} \sim Gau(T_i^{(t)}, \sigma_{y,i}^{(t)2})$, or [19]

$$p\left(Y_i^{(t)}\middle|T_i^{(t)},X\right) \propto \exp\left\{-\frac{\left[Y_i^{(t)} - T_i^{(t)}(X)\right]^2}{2\sigma_{y,i}^{(t)2}}\right\} \tag{2}$$

Similarly, the likelihood of the modeled data can be written as [19]

$$p\left(T_i^{(t)}|X\right) \propto \exp\left\{-\frac{\left[T_i^{(t)}(X) - F_i^{(t)}(X)\right]^2}{2\sigma_{f,i}^{(t)2}}\right\} \tag{3}$$

Since unsteady inversion model is discussed here, all the concentration data will depend on the time. It is different from the original work by Chow et al. [18] and Keats et al. [19], the likelihood function needs to be deduced and restudied considering time issue.

If the measurement error and model error at any sensor at any time are assumed to be independent, the likelihood function can be written as follows:

$$p(Y|X) = \prod_{t=1}^{n}\prod_{i=1}^{k} p\left(Y_i^{(t)}|X\right) \propto \exp\left\{-\sum_{t=1}^{n}\sum_{i=1}^{k}\frac{\left[F_i^{(t)}(X) - Y_i^{(t)}\right]^2}{2\left[\sigma_{f,i}^{(t)2} + \sigma_{y,i}^{(t)2}\right]}\right\} \tag{4}$$

Substituting (4) to (1), the posterior distribution of the source term X can be obtained as follows:

$$p(X|Y) \propto p(X) \exp\left\{ -\sum_{t=1}^{n}\sum_{i=1}^{k} \frac{\left[F_i^{(t)}(X) - Y_i^{(t)}\right]^2}{2\left[\sigma_{f,i}^{(t)2} + \sigma_{y,i}^{(t)2}\right]} \right\} \Big/ p(Y) \tag{5}$$

where

$$p(Y) = \int p(Y|X)p(X)dX \propto \int \exp\left\{ -\sum_{t=1}^{n}\sum_{i=1}^{k} \frac{\left[F_i^{(t)}(X) - Y_i^{(t)}\right]^2}{2\left[\sigma_{f,i}^{(t)2} + \sigma_{y,i}^{(t)2}\right]} \right\} p(X)dX \tag{6}$$

2.3. Markov Chain Monte Carlo sampling

Up to now, the final form of the posterior possibilities of the source term has been obtained. However, if the posterior possibilities are computed according to Eq. (5), the integral throughout the entire domain of the parameter space has to be evaluated numerically using Eq. (6). Considering the dimensionality of the source term **X** is large, and the computation involved forward simulation $F_i^{(t)}(\mathbf{X})$ is also time-consuming, the calculation using Eq. (5) is prohibitively expensive. An alternative method is to use the Markov chain technique to generate a collection of realization which has the posterior distribution of the source term as its limiting stationary distribution. The samples in the chain can then be used to conduct inference. Detailed implementation of the sampling algorithm is described in [18,20].

2.4. Unsteady adjoint equation

From Eq. (5), numerical predicted concentrations $F_i^{(t)}(X)$ at the given sensor (monitor) sites at prescribed time points for the given source term parameters are necessary to obtain the likelihood function. The unsteady advection-diffusion equation for concentration must be therefore solved.

$$\begin{cases} \frac{\partial C}{\partial t} + \vec{V}\cdot\nabla C - \nabla\cdot(D\nabla C) = S \quad X \in \Omega \\ b.c. \nabla C\cdot\vec{n} = 0 \quad X \in \partial\Omega \\ i.c. C(X, t=0) = 0 \end{cases} \tag{7}$$

It is assumed that the concentration field has no impact on the velocity field, Eq. (7) is therefore a linear one. The concentration $F_i^{(t)}(X_s)$ at the given sensor site R_i at time t can then be broken down into additive contributions from each time interval [20]:

$$F_i^{(t)}(X_s) = \sum_{t_k=t_0}^{t} C'(R_i, X_s, t, t_k)Q \tag{8}$$

where $C'(R_i,X_s,t,t_k)$ denotes the concentration at the given sensor site R_i at time t due to a unit point source release at the location X_s within the time interval (t_{k-1},t_k), and Q is the source release rate.

To avoid repeated computation during the sampling and make the inversion efficient, before MCMC sampling, we need to solve Eq. (7) for all the possible source parameters and store the solutions in a database. That is to say, one forward simulation has to be carried out for each of the possible combinations of source location and strength. Generally there are more than thousands of combinations. The traditional approach is to solve the unsteady advection-diffusion Eq. (7) enormous times to obtain all the possible solution $F_i^{(t)}(X_s)$. The calculation is extremely time-consuming.

Considering the number of the sensors is much less than that of the possible source locations, Keats et al. [19] solved an adjoint advection-diffusion equation. Although the computational time is nearly the same for original and adjoint equations, the adjoint equation need to be solved only once for each sensor, which makes the amount of calculation reduced dramatically. In this paper an unsteady dispersion process and dynamic source inversion are discussed, and unsteady adjoint advection-diffusion equation [19] is applied to improve the computing efficiency. The relationship between forward concentration and adjoint concentration considering time issue are deduced in detail as follows.

$$\begin{cases} \frac{\partial G}{\partial \tau} - \vec{V}\cdot\nabla G - \nabla\cdot(D\nabla G) = \delta(X - X', \tau) \quad X \in \Omega \\ b.c. G\vec{V}\cdot\vec{n} + D\nabla G\cdot\vec{n} = 0 \quad X \in \partial\Omega \\ i.c. G(X, \tau = 0) = 0 \end{cases} \tag{9}$$

Substituting Eq. (9) into

$$C(X', t') = \int_0^{t'} dt \int_\Omega C(X, t)\delta(X - X', t - t')dX \tag{10}$$

and defining a new time $t = t' - \tau$, we obtain:

$$C(X', t') = \int_0^{t'} d\tau \int_\Omega C\left(\frac{\partial G}{\partial \tau} - \vec{V}\cdot\nabla G - \nabla\cdot(D\nabla G)\right)dX \tag{11}$$

Using the incompressible condition and vector relations:

$$C(X', t') = \int_0^{t'} dt \int_\Omega \left[-\frac{\partial CG}{\partial t} + GS - \nabla\cdot(CG\vec{V}) - \nabla\cdot(CD\nabla G) + \nabla\cdot(DG\nabla C)\right]dX \tag{12}$$

Through the divergence theorem, Eq. (12) can be written as:

$$C(X', t') = \int_0^{t'} dt \int_\Omega \left[-\frac{\partial CG}{\partial t} + GS\right]dX - \int_0^{t'} dt \int_{\partial\Omega} (CG\vec{V} + CD\nabla G - DG\nabla C)\cdot\vec{n}d\Gamma \tag{13}$$

Substituting $\nabla C\cdot\vec{n} = 0, G\vec{V}\cdot\vec{n} + D\nabla G\cdot\vec{n} = 0 X \in \partial\Omega, G(X, t' = 0) = 0$ and $C(X,t=0) = 0$ into Eq. (13), and considering a point source continuous release [19]:

$$C(X', t') = \int_0^{t'} Q(t)\cdot G(X_s, X', t' - t, 0)dt \tag{14}$$

The solution of Eq. (7) can then be expressed in terms of the solution of the adjoint Eq. (9). Similar to Eq. (8), the concentration at the given sensor site R_i at the given time point t can be given as follows:

$$F_i^{(t)}(X_s) = \sum_{\tau_k=t_0}^{t} G(X_s, R_i, t - \tau_k, 0)Q(\tau_k)\Delta\tau_k \tag{15}$$

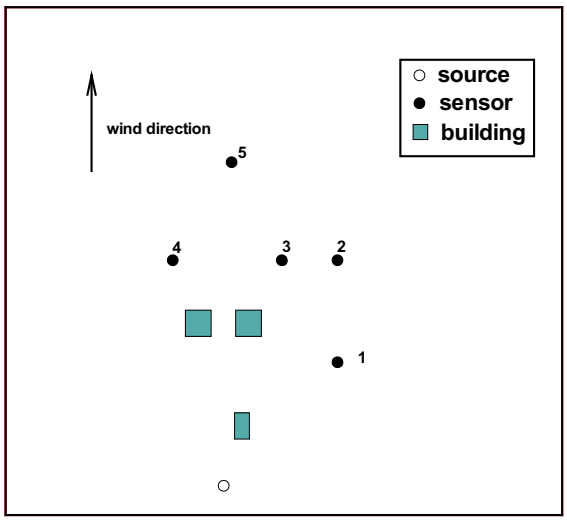

Fig. 1. The schematic of the buildings, source and sensors (planform).

where $G(X_s,R_i,t-\tau_k,0)$ denotes the adjoint concentration at the location X_s at the given time point $t-\tau_k$ due to a unit point source release instantaneously at the sensor site R_i at the initial time.

In order to obtain the concentrations at the given sensor site R_i at the given time point t due to the source release at different locations:

$$(X_{s1}, X_{s2}, \cdots, X_{sk}, \cdots, X_{sn})$$

The unsteady advection-diffusion Eq. (7) has to be solved n times, if (8) is used, while the unsteady adjoint Eq. (9) needs to be solved only once, if (15) is used.

3. Results and discussion

3.1. Case description

In this case, the source inversion of an unsteady dispersion process of the hazardous CBR materials release in a three-dimensional urban environment is investigated. The dimension of the whole domain is 500 m × 500 m × 100 m as shown in Fig. 1. There are three buildings (cuboids) in this domain with dimensions of 30 m × 30 m × 25 m, 30 m × 30 m × 25 m and 20 m × 30 m × 20 m respectively. A point source located upwind from the buildings starts to release at a given time with a release rate of 0.8 kg/m^3 s. Its position coordinate is (−50 m, − 225 m,5 m) (The origin of the coordinate axis is placed at the center of the domain). The distance between the source and its nearest building is 55 m. Five sensors located in this domain can record the atmospheric concentrations and report the data every 10 s. Each sensor provides time-dependent concentrations for a total of seven 10-s intervals from 30 s to 100 s. The wind speed is 5 m/s. The wind direction parallels the y axis. Both sensor and model errors exist. In this paper, two errors are incorporated into one error parameter σ, and $\sigma^2 = \sigma_f^2 + \sigma_y^2$ (in this case, $\sigma = 0.4$), see [21]. The error distribution is assumed to be steady.

3.2. Forward numerical model

According to the analysis of aforementioned Section 2.4, unsteady adjoint Eq. (9) needs to be solved for each of possible source parameters and results should be stored in a database before MCMC sampling. Before it, the flow field around the buildings should be solved. A three-dimensional incompressible time-dependent flow code based on Cartesian grids, Gerris [22], is employed to solve the Navier–Stokes equations and concentration scalar equation. In this code, the second-order approximate projection method based on the collocated grid [23,24] is adopted. Details are described in [22]. The code is applied to simulate atmospheric flow around obstacles within a large spatial domain and validated by comparing with experimental measurements [25].

To improve the efficiency and accuracy, adaptive mesh refinement technique in Gerris is adopted. In our case, two refinement criterions are used, based on the norm of the local vorticity and the gradient of the adjoin concentration to adjust the grids dynamically. All of the cells which do not satisfy the refinement criterion are coarsened, otherwise refined. Fig. 2 shows the adapted grids on a horizontal plane ($z = 0$) at different times. The spatial resolution is about 0.97 m near the buildings and is adapted down to a maximum scale of 25 m in the z direction. And the number of grids is decreased from 267,934 to 46,269 dynamically.

According to Section 2.4, an unsteady concentration database for all possible source locations need to be generated before MCMC sampling. If using the original concentration Eq. (7), the simulation has to be performed 131,220 times because the source location space is discretised to 81 × 81 × 20 grids, while the adjoint concentration Eq. (9) need to be solved only five times since there are five sensors. The ratio of computation between two methods is about 131220:5. The computation is therefore efficient by using adjoint concentration equation. Fig. 3 shows the temporal variation of the concentration at five sensors due to a unit point source releases at the actual location through solving the adjoint Eq. (9). In order to make comparison, the figure also shows the concentration predicted by solving the original forward concentration Eq. (7). From the figure we can see that the concentrations predicted by the adjoint Eq. (9) agree well with those by the forward concentration Eq. (7).

3.3. Inversion results

The Markov chain is initialized at the center of the domain, and converged to the vicinity of the actual source location after a burn-in period. The length of the whole Markov chain is 40,000. To make it a fully mixing chain and 'forget' its starting point, the first half of the samples (20,000 iterations) are discarded and the second half of the chain is used to make the inference.

Samples from the MCMC algorithms are usually autocorrelated, due to the inherent Markovian dependence structure. The degree of autocorrelation can be quantified using autocorrelation function:

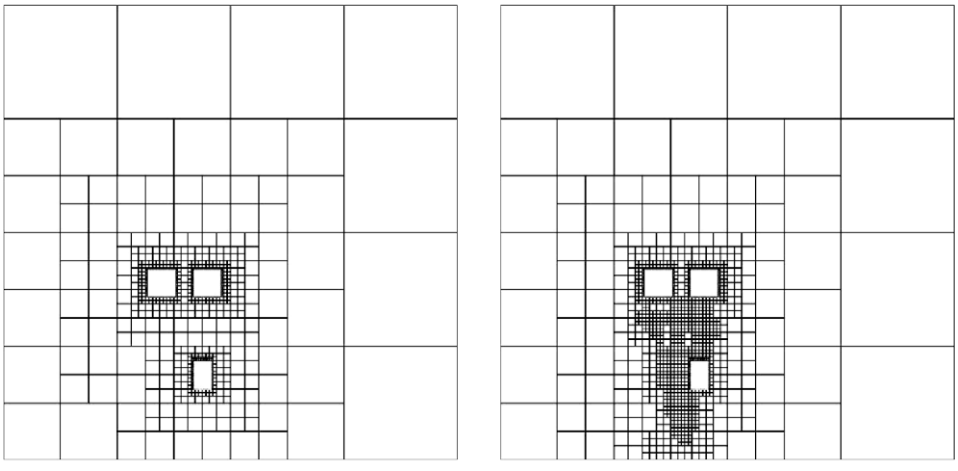

(a) 10s (b) 100s

Fig. 2. The adapted grids on a horizontal plane at (a) 10 s and (b) 100 s.

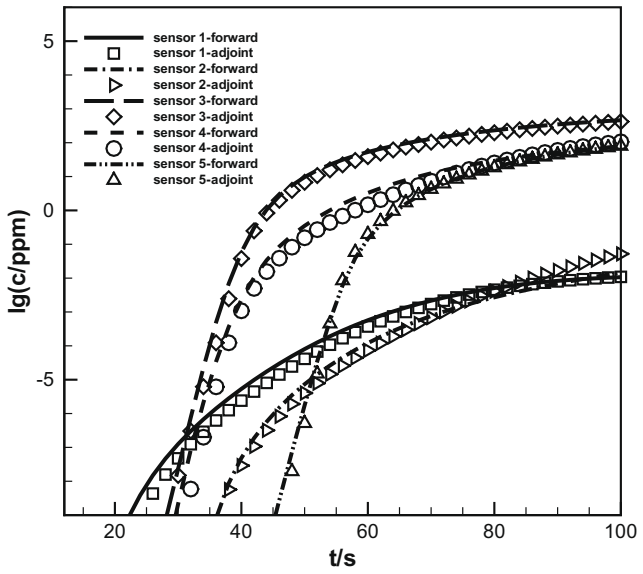

Fig. 3. Comparison of temporal variation of concentration at five sensors using forward equation and adjoint equation.

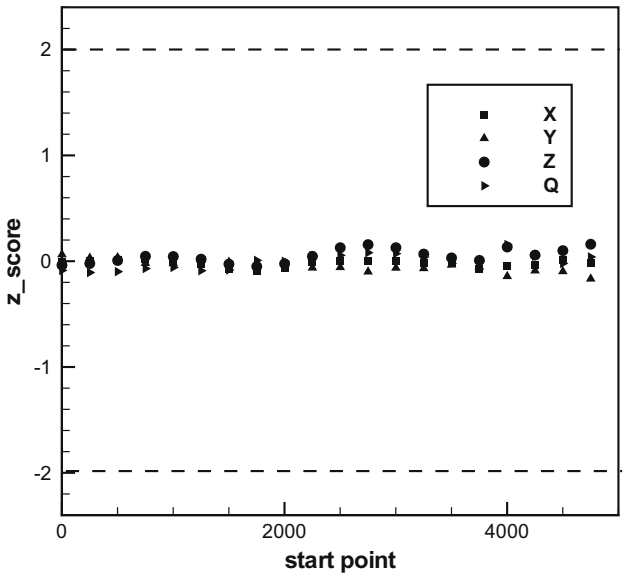

Fig. 5. *z_score* for various initial segments along the Markov chain.

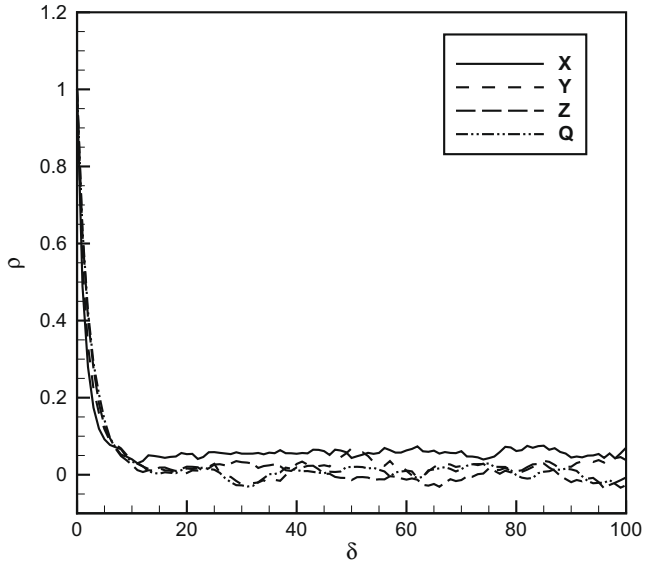

Fig. 4. The autocorrelation plots for source parameter.

$$\rho = \frac{Cov(X_t, X_{t+\delta})}{\sqrt{var(X_t)\,var(X_{t+\delta})}} = \frac{E[(X_t-\theta)(X_{t+\delta}-\theta)]}{\sqrt{E\left[(X_t-\theta)^2\right]E\left[(X_{t+\delta}-\theta)^2\right]}} = \frac{\sum_{i=0}^{N-\delta-1}(X_{i+\delta}-\bar{X})(X_i-\bar{X})/(N-\delta)}{\sum_{i=0}^{N-1}(X_i-\bar{X})^2/N} \quad (16)$$

Significant autocorrelation suggests the chain need thinning every δ samples prior to use of the posterior statistics for inference. Fig. 4 shows the degree of autocorrelation ρ as a function of thinning interval δ in the Markov chain, and from the figure, the autocorrelation is small enough to conduct inference when the interval δ is larger than 20.

The statistical convergence to the posterior distribution for the Markov chain is detected using a time-series approach, first proposed by Geweke [26], which compares the mean and variance of the segments from the beginning and the end of the single chain.

$$z\_score = \frac{\bar{X}_a - \bar{X}_b}{\sqrt{var(X_a) + var(X_b)}} \quad (17)$$

where X_a is the chain with the early segment and X_b is the chain with the late segment. If *z_score* of these two segments are similar and fall within 2 standard deviation of zero, it can provide the evidence for convergence. Fig. 5 shows *z_score* of the difference between various initial segments and the last half of the remaining chain. The label on the x axis in the figure denotes the start point of initial segment X_a. From the figure, the majority of points fall within 2 standard deviation of zero, indicating that the sampling points are proper to generate the posterior distribution of source parameters.

The posterior probabilities of the source parameters are shown in Fig. 6, using the histogram plots, which quantified the marginal probability distributions of the source locations (x,y,z) and its strength. From four figures, the peaks of the histograms are all located in the vicinity of actual source parameters. Fig. 7 shows two-dimensional joint probability distributions of the source location on three planes which are $z = 5$ m, $y = -225$ m, $x = -50$ m respectively along with the location of sensors and the true location of the source. The peaks of the joint probability distributions on three planes also coincide with the actual location of the source. Fig. 8 shows the 80% confidence contour of the source location, indicating that 80% confidence that the source is located within the iso-surface. The probabilistic predictions of the source location with a certain confidence are more important for emergency manager than an optimal source location without any uncertainty analysis using the optimization approach.

Table 1 shows the summary statistics of the source parameters generated from the MCMC samples. The posterior expectation (mean) of the source parameters are close to the actual value. The largest location deviation is less than 2 m with the relative error 3.8%. And the mean of the strength deviation is 0.015 kg/m^{3}s with the relative error 1.8%. The standard deviation in y direction is larger than those in other directions, indicating that the y of the source location can be more uncertain, since a weaker source closer to the sensor in the wind direction can generate similar concentrations to a stronger source far away from the sensors. This conclusion is the same as that made by Chow [18]. Because the time-dependent concentration informa-

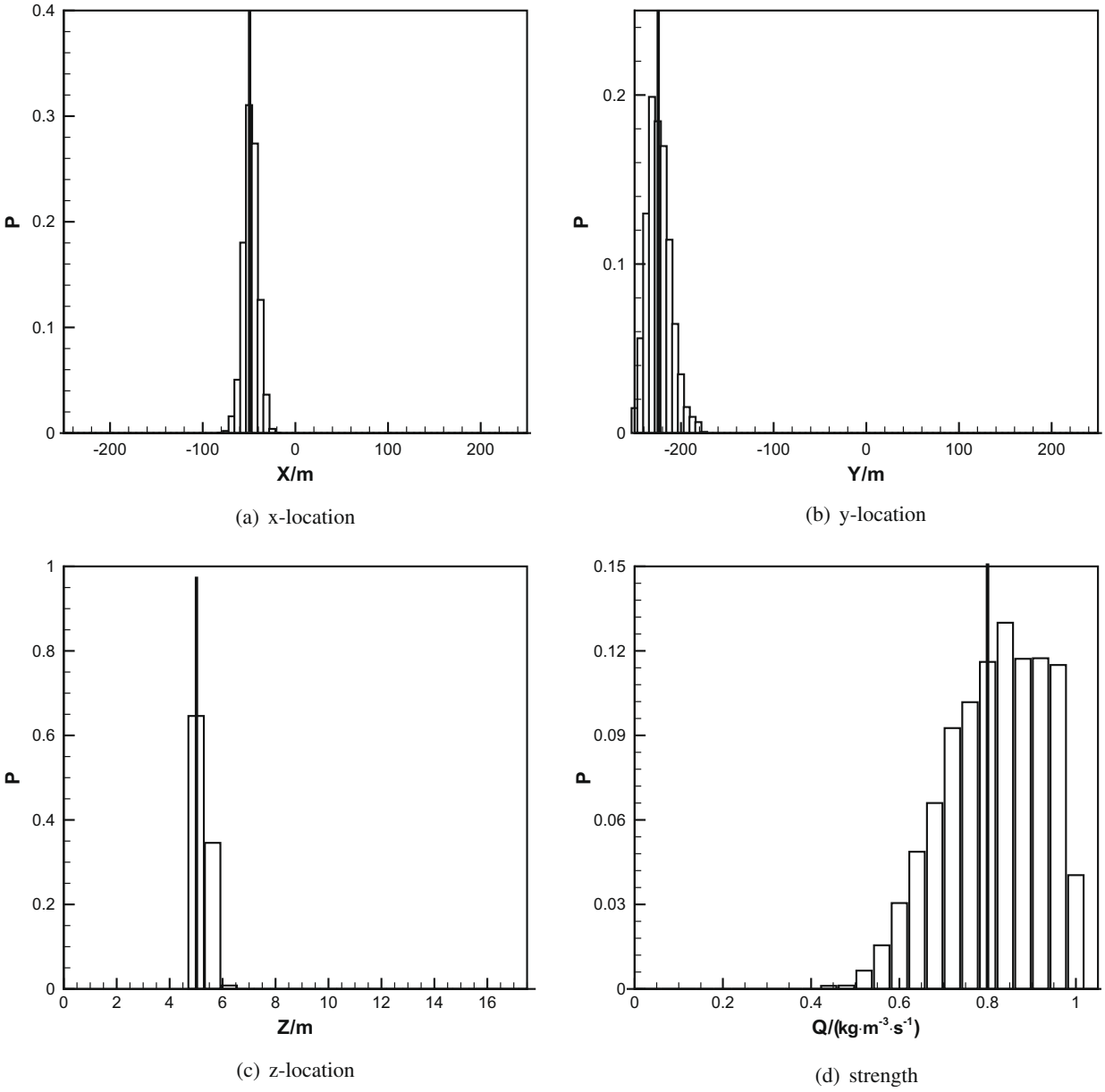

(a) x-location (b) y-location

(c) z-location (d) strength

Fig. 6. The histogram of source parameters, with the actual value shown as the vertical line.

tion is added, compared with the steady reversion (the mean deviation is 6.4 m and the standard deviation is 22.1 m, see our previous work), unsteady reversion method can improve the accuracy of source location in the wind direction.

3.4. Model check using posterior predictive simulation

Since the draws $X = \{X^{(1)}, X^{(2)}, \cdots, X^{(t)}, \cdots, X^{(n)}\}$ from the posterior distribution using the Markov chain simulation have been obtained, a Bayesian test of model fit using the posterior predictive distribution proposed by Gelman et al. [27] can be employed.

The sampling distribution of measurement data Y^{rep} given the source parameters can be written as follows:

$$p(Y^{rep}|Y) = \int p(Y^{rep}|X)p(X|Y)dX \tag{18}$$

Then N hypothetical replications of the data

$$Y_k^{rep} = \left\{ Y_k^{rep,(1)}, Y_k^{rep,(2)}, \cdots, Y_k^{rep,(t)}, \cdots, Y_k^{rep,(n)} \right\}$$

can be drawn from this distribution. If the model is reasonably accurate, the hypothetical replications of the data from the Markov chain of the source parameters should look similar to the observed data Y.

Since the number of the observed data is large, we choose a function $T(Y^{rep}) = \sum_{k=1}^{n} Y_k^{rep}/n$, the average of the measurement data instead of Y itself, as the discrepancy variable to perform the posterior predictive model check. Then a p-value can be estimated by calculating the proportion of the cases in which the simulated discrepancy variable exceeds the observed data.

$$p - \text{value} = \frac{1}{N}\sum_{i=1}^{N} I[T(Y^{rep,(i)}) \geqslant T(Y)] \tag{19}$$

where I is the function which takes 1 when the argument is true and 0 otherwise. This measure compares the deviance of the observed data from the actual source parameters to deviance of the simulated

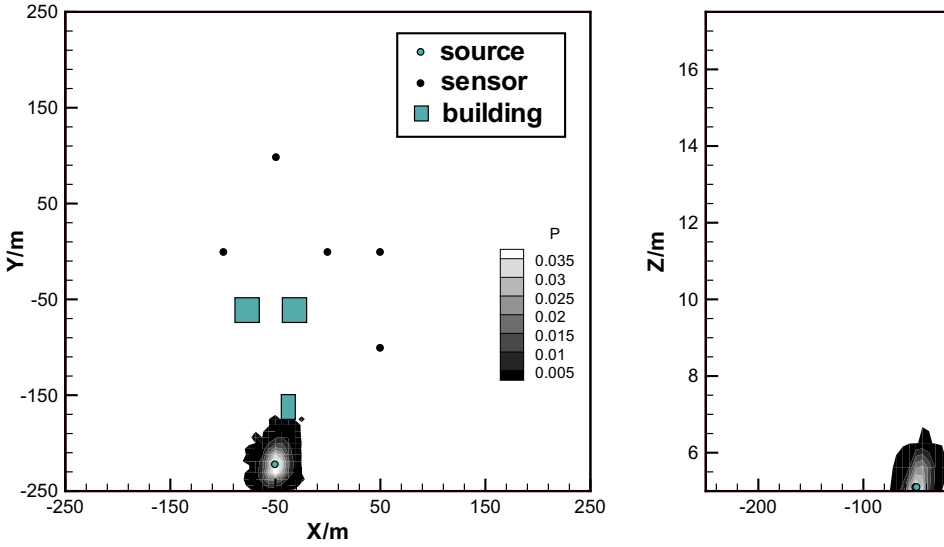

(a) z=5m

(b) y=-225m

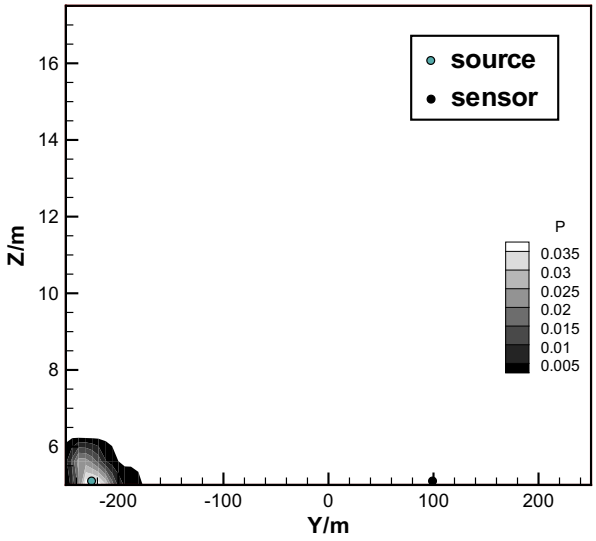

(c) x=-50m

Fig. 7. The two-dimensional joint probability distributions of the source location on the plane.

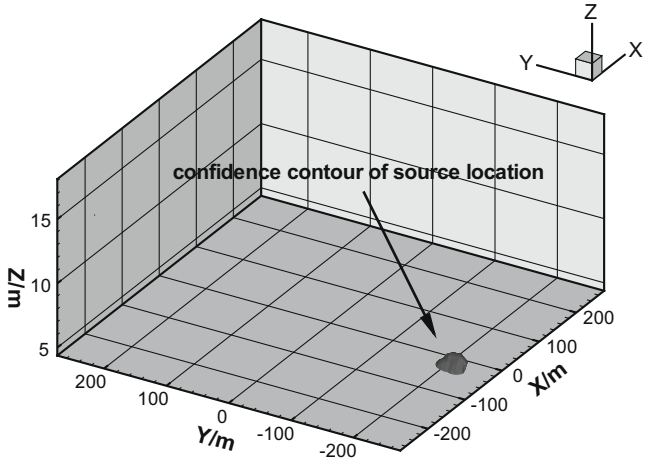

Fig. 8. The 80% confidence region of the source location.

Table 1
The summary statistics of the source parameters.

Parameters	True	Mean	Standard deviation
x/m	−50	−48.03	7.98
y/m	−225	−223.56	12.91
z/m	5	5.90	1.24
$Q/(\mathrm{kg\,m^{-3}\,s^{-1}})$	0.80	0.815	0.112

data from the trace of the source parameters. So the p-value should be close to 0.5 for a well-fit model.

Fig. 9 shows the histogram of $T(Y^{rep})$ using the hypothetical replications of the data from the Markov chain of the source parameters, with the observed data $T(Y)$, indicated by the vertical line. From the figure, the observed data $T(Y)$ is very close to the peak of the posterior prediction distribution, with the p-value 0.46, computed using (27), which indicates that the model is very good fit.

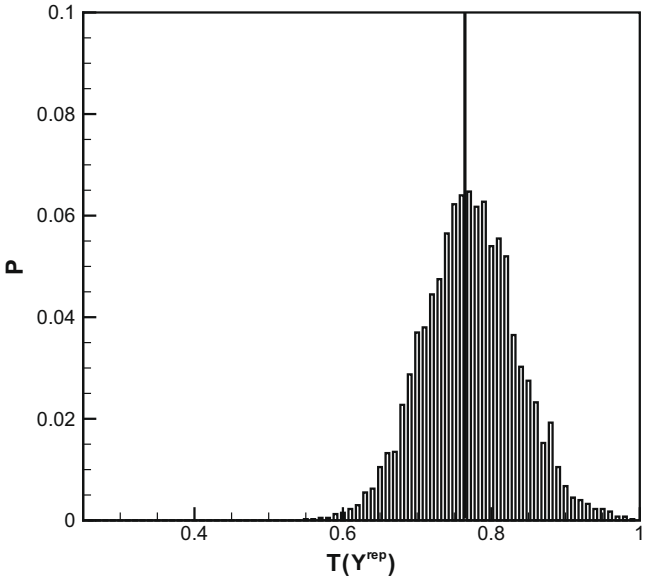

Fig. 9. The histogram of discrepancy variable.

4. Conclusions

Unsteady dispersion of hazardous CBR materials release in three-dimensional urban environment has been simulated. The Bayesian probabilistic approach along with the Markov Chain Monte Carlo sampling and unsteady adjoint transportation equation based on adaptive mesh refinement technique have been adopted to determine and identify the location and strength of the source. Successful dynamic inversion indicates the feasibility of the proposed method and procedure. From the results, the peaks of the marginal probability distributions and the joint probability distributions on three planes are all coincide with the actual source parameters. The largest deviation for the mean of the source location is less than 2 m with the relative error 3.8%, while the mean of the strength deviation is 0.015 kg/m^3 s with the relative error 1.8%. Meanwhile, model check using posterior predictive simulation also shows the inversion model is very well fit. In addition, using the unsteady adjoint advection-diffusion equation and adaptive mesh refinement technique, the computation is more efficient especially in the unsteady inversion process. We also found that unsteady inversion method can improve the accuracy of source location in the wind direction compared with the steady inversion method, since concentration value at different time sampling points can be added sequentially in the inversion process. In our previous steady inversion case, the standard deviation of source location in wind direction is 22.1 m, while using unsteady inversion, the standard deviation is reduced to 12.91 m. Thus the time-dependent concentration information can be used to reduce uncertainty in source location prediction.

Acknowledgement

This work is supported by the National Natural Science Foundation of China (NSFC), No. 50804027.

References

[1] N.K. Arystanbekova, Application of Gaussian plume models for air pollution simulation at instantaneous emissions, Math. Comput. Simul. 67 (4–5) (2004) 451–458.
[2] J.E. Flaherty, D. Stock, B. Lamb, Computational fluid dynamic simulations of plume dispersion in urban Oklahoma City, J. Appl. Meteorol. Climatol. 46 (12) (2007) 2110–2126.
[3] S.V. Patankar, D.B. Spalding, A calculation procedure for heat, mass and momentum transfer in three-dimensional parabolic flows, Int. J. Heat Mass Transfer 15 (10) (1972) 1787–1806.
[4] B.E. Launder, D.B. Spalding, The numerical computation of turbulent flows, Comput. Meth. Appl. Mech. Eng. 3 (2) (1974) 269–289.
[5] I.G. Enting (Ed.), Inverse Problems in Atmospheric Constituent Transport, Cambridge University Press, Cambridge, 2002.
[6] R.G. Hills, G.P. Mulholland, The accuracy and resolving power of one dimensional transient inverse heat conduction theory as applied to discrete and inaccurate measurements, Int. J. Heat Mass Transfer 22 (8) (1979) 1221–1229.
[7] M. Monde, Analytical method in inverse heat transfer problem using Laplace transform technique, Int. J. Heat Mass Transfer 43 (21) (2000) 3965–3975.
[8] O.R. Burggraf, An exact solution of the inverse problem in heat conduction theory and application, J. Heat Transfer 86 (1964) 373–382.
[9] C.Y. Yang, The determination of two heat sources in an inverse heat conduction problem, Int. J. Heat Mass Transfer 42 (2) (1999) 345–356.
[10] F. Lefevre, C. Le Niliot, Multiple transient point heat sources identification in heat diffusion: application to experimental 2D problems, Int. J. Heat Mass Transfer 45 (9) (2002) 1951–1964.
[11] C. Le Niliot, F. Lefevre, A parameter estimation approach to solve the inverse problem of point heat sources identification, Int. J. Heat Mass Transfer 47 (4) (2004) 827–841.
[12] J.V. Beck, B. Blackwell, C.R.S. Clair (Eds.), Inverse Heat Conduction, Wiley-Interscience, New York, 1985.
[13] N. Daouas, M.S. Radhouani, A new approach of the Kalman filter using future temperature measurements for nonlinear inverse heat conduction problems, Numer. Heat Transfer B 45 (6) (2004) 565–585.
[14] S. Deng, Y. Hwang, Solution of inverse heat conduction problems using Kalman filter-enhanced Bayesian back propagation neural network data fusion, Int. J. Heat Mass Transfer 50 (11-12) (2007) 2089–2100.
[15] E.H. Shiguemori, J.D.S. Da Silva, H.F.D. Velho, Estimation of initial condition in heat conduction by neural network, Inverse Prob. Sci. Eng. 12 (3) (2004) 317–328.
[16] J.B. Wang, N. Zabaras, A Bayesian inference approach to the inverse heat conduction problem, Int. J. Heat Mass Transfer 47 (17-18) (2004) 3927–3941.
[17] J.B. Wang, N. Zabaras, A Markov random field model of contamination source identification in porous media flow, Int. J. Heat Mass Transfer 49 (5-6) (2006) 939–950.
[18] F.K. Chow, B. Kosovic, S.T. Chan, Source inversion for contaminant plume dispersion in urban environments using building-resolving simulations, in: American Meteorological Society's 6th Symposium on the Urban Environment, Atlanta, 2006.
[19] A. Keats, E. Yee, F.S. Lien, Bayesian inference for source determination with applications to a complex urban environment, Atmos. Environ. 41 (3) (2007) 465–479.
[20] G. Johannesson, B. Hanley, J. Nitao, Dynamic bayesian models via Monte Carlo – an introduction with examples, Technical report UCRL-TR-20717, Lawrence Livermore National Laboratory, Livermore CA, 2004.
[21] J.K. Lundquist, B. Kosovic, R. Belles, Synthetic event reconstruction experiments for defining sensor network characteristics, Technical report UCRL-TR-217762, Lawrence Livermore National Laboratory, Livermore CA, 2005.
[22] S. Popinet, Gerris: a tree-based adaptive solver for the incompressible Euler equations in complex geometries, J. Comput. Phys. 190 (2) (2003) 572–600.
[23] D.F. Martin, P. Colella, A cell-centered adaptive projection method for the incompressible Euler equations, J. Comput. Phys. 163 (2) (2000) 271–312.
[24] J.B. Bell, P. Colella, H.M. Glaz, A 2nd-order projection method for the incompressible Navier–Stokes equations, J. Comput. Phys. 85 (2) (1989) 257–283.
[25] S. Popinet, M. Smith, C. Stevens, Experimental and numerical study of the turbulence characteristics of airflow around a research vessel, J. Atmos. Ocean. Technol. 21 (10) (2004) 1575–1589.
[26] J. Geweke, Evaluating the accuracy of sampling-based approaches to the calculation of posterior moments, in: J.M. Bernardo, J. Berger, A.P. Dawid, A.F.M. Smith (Eds.), Bayesian Statistics 4, Oxford University Press, Oxford, 1992, pp. 169–193.
[27] A. Gelman, X.L. Meng, Model checking and model improvement, in: W.R. Gilks, S. Richardson, D.J. Spiegelhalter (Eds.), Markov Chain Monte Carlo in Practice, Chapman and Hall, London, 1996, pp. 189–201.